

**CONCEPTUAL STUDY OF AN “ANTI-TAGGED” EXPERIMENT  
SEARCHING FOR  $\nu_\mu \rightarrow \nu_e$  OSCILLATION**

Lucio Ludovici<sup>1)</sup>, Piero Zucchelli  
CERN, CH-1211 Geneva 23, Switzerland

**Abstract**

We study the conceptual feasibility of a high energy, “short baseline”, zero background experiment to search for  $\nu_\mu \rightarrow \nu_e$  oscillations and fully covering the area where the LSND experiment claims evidence. The natural  $\nu_e$  background of the  $\nu_\mu$  beam, from  $K$  and  $\mu$  decays in the decay tunnel, is suppressed by a hadron blind detector that vetoes, by time coincidence, a possible  $\nu_e$  signal in the neutrino detector (*anti-tagging technique*). We discuss this new idea and we study a possible implementation in the old neutrino line of the PS accelerator, which at CERN offers the ideal  $L/E$  ratio. In the anti-tagged  $\nu_\mu$  beam, the  $\nu_e$  contamination can be reduced by more than two orders of magnitude over conventional beams, down to  $\nu_e/\nu_\mu = 5 \cdot 10^{-5}$ . In an ideal appearance experiment using a 300  $t$  detector one would expect after two years 112 events according to the LSND result, with a background of  $1.1 \div 2.4$  events. In case of a negative search, the 90% C.L. upper limit in the mixing angle would be  $\sin^2 2\theta_{e\mu} < 1.8 \cdot 10^{-4}$  for large  $\Delta m_{e\mu}^2$  and  $\Delta m_{e\mu}^2 < 3.3 \cdot 10^{-2} eV^2$  for maximal mixing.

(Submitted to *Nucl. Instr. and Methods A*)

---

<sup>1)</sup> On leave from INFN, Sezione di Roma “La Sapienza”, Rome, Italy

## 1 Physics Motivations

In the current experimental scenario of the neutrino oscillation search, claims of positive results come from the solar  $\nu_e$  deficit [1, 2, 3, 4], the atmospheric anomalous  $\nu_\mu/\nu_e$  ratio [5, 6], and the LSND  $\bar{\nu}_e$  excess [7]. Whether the solar neutrino problem should be attributed to neutrino oscillations [8, 9] or to the solar properties [10, 11, 12, 13] is still an open question. On the atmospheric neutrino anomaly, different results [14, 15, 16] and interpretations [17, 18] suggest a conservative attitude in drawing definite conclusions. SuperKamiokande [19] will provide soon an order of magnitude increase of the data available to study the atmospheric neutrino deficit and, with SNO [20] and BOREXINO [21], a deeper insight into the solar neutrino problem. On the other hand, no present or approved experiment is going to encompass the area indicated by LSND for possible  $\nu_\mu \rightarrow \nu_e$  oscillations. In the coming years, LSND will continue taking data and the KARMEN experiment, after an upgrade to provide a better shield for cosmic rays[22], should reach a sensitivity comparable to that of LSND. It should be noted however that both experiments have a similar neutron signature in the same energy range and rely on background subtraction from similar sources. Furthermore, the LSND present analysis of the data [23] shows a limited potential in measuring the  $\Delta m_{e\mu}^2$  parameter.

The variety of theoretical models [9, 24, 25, 26, 27] predicting incompatible values of neutrino masses and mixing angles and the lack of a compelling experimental indication, strengthen the belief that future experiments should be mostly motivated by

- a *discovery potential* which should allow to confirm or disprove existing claims of evidence for oscillation with a larger significance, possibly with a different detection technique and experimental signature;
- an *experimental sensitivity* which in case of a negative result should allow to exclude a large and still unexplored area of at least one or two orders of magnitude in the  $\Delta m^2$  and  $\sin^2 2\theta$  plane.

The subject of this paper is the feasibility of a high energy beam ( $E_\nu \gtrsim 1$  GeV), short baseline appearance  $\nu_\mu \rightarrow \nu_e$  experiment with “zero background” and maximum sensitivity for  $\Delta m_{e\mu}^2 \approx \text{few } eV^2$ . This offers a unique opportunity to probe the region where LSND claims evidence for oscillation with a different signature, ultimately measuring the  $\Delta m_{e\mu}^2$  parameter in case of positive evidence.

The main problem to face using high energy  $\nu_\mu$  beams consists in the irreducible background due to  $\nu_e$  contamination produced by kaon and muon decays in the decay tunnel. In conventional neutrino beams and detector setups [28, 29, 30, 31], the expected  $\nu_e$  events due to the beam contamination are of the order of 0.5 – 2% with respect to the  $\nu_\mu$  interactions and this makes it very difficult to probe the oscillation probability  $P(\nu_\mu \rightarrow \nu_e) = (0.31_{-0.10}^{+0.11} \pm 0.05)\%$  given by LSND.

## 2 Motivation for a zero background experiment

The search for  $\nu_\mu \rightarrow \nu_e$  oscillation in the appearance mode in a conventional  $\nu_\mu$  beam requires an accurate modelling of the small  $\nu_e$  content in order to subtract the corresponding background. In the regime where a *large background* from  $\nu_e$  contamination has to be subtracted, the 90% C.L. limit put on the oscillation probability by a negative search in an appearance experiment is ideally<sup>1)</sup> given by

$$P(\nu_\mu \rightarrow \nu_e) \simeq 1.28 \sqrt{\frac{C_e}{N} \left( 1 + \frac{(\Delta C_e)^2}{C_e} N + C_e \right)} \quad (1)$$

---

<sup>1)</sup> All other background contributions are neglected.

where  $N$  is the observed number of neutrino interactions,  $C_e$  is the  $\nu_e$  contamination of the beam and  $\Delta C_e$  is its absolute uncertainty.

In a *zero background* experiment, which could be defined by the condition  $C_e N \lesssim 1$ , the limit on the oscillation probability is given by

$$P(\nu_\mu \rightarrow \nu_e) = \frac{2.3}{N} \gtrsim 2.3 \cdot C_e \quad (2)$$

To give a numerical example, in a conventional beam with a  $\nu_e$  contamination  $C_e = 1\%$  and  $\Delta C_e/C_e = 3\%^{(2)}$ , as long as the *zero background* condition is valid, the limit improves like  $1/N$ . Then, below  $P(\nu_\mu \rightarrow \nu_e) \approx 2.3 \cdot C_e = 2.3 \times 10^{-2}$ , the limit improves only as  $1/\sqrt{N}$  up to the asymptotic limit  $P(\nu_\mu \rightarrow \nu_e) \approx 1.28 \cdot \Delta C_e = 3.8 \times 10^{-4}$ , which is reached for

$$N \gtrsim \frac{(1 + C_e)C_e}{\Delta C_e^2} \quad (3)$$

In the example above this would correspond to  $N \gtrsim 1.1 \times 10^5$ .

In other terms, an experiment taking  $N = 100,000$  events in such a beam could set a limit  $P(\nu_\mu \rightarrow \nu_e) = 5.6 \times 10^{-4}$  while the same limit could be obtained with  $N = 4100$  events by a *zero background* experiment. This experiment would require a reduction of the  $\nu_e$  contamination to  $C_e \lesssim 1/N = 2.4 \times 10^{-4}$ . An ideal neutrino detector in a *zero background* beam would then reach the same limit set by a detector  $\sim 25$  times larger in a beam with the  $\nu_e$  contamination stated above.

From the point of view of studying the properties of a possible signal (like the oscillation parameter  $\Delta m_{e\mu}^2$ ) a *zero background* experiment offers the advantage of a clear *event by event* identification of the signal, while in presence of background any information about the signal has to be extracted statistically from the candidate events.

### 3 Anti-tagging Principle

The principle of the anti-tagging consists in a delayed time coincidence between the  $\nu_e$  production time in the meson decay and its interaction time in the neutrino detector. With respect to the existing idea of a *tagged neutrino beam* [32, 33], the flavour identification is restricted to the  $\nu_e$  background events and the neutrino detector can be at any distance from the source because no spatial correlation between the decay and the interaction is required.

The aim of the anti-tagging is to suppress the  $\nu_e$  contamination installing in the decay tunnel a detector capable to identify the production of each  $\nu_e$ , thus vetoing the interactions which occur in the neutrino detector. Indeed, the tagging detector measures the positron accompanying the neutrino in the decay  $M \rightarrow \nu_e e^+ X$ . In figure 1 is depicted the schematic arrangement of the experiment. Thin, planar modules installed in the decay tunnel perpendicularly to the meson beam, detect the passage of the positron measuring its crossing time  $T_e(i)$  on the  $i$ -th module. A downstream detector records all neutrino events and measures their interaction time  $T_{\nu D}$ .

Given a neutrino interaction, the information of all tagging modules is recorded in order to look for possible positron signals at time

$$T_e(i) = T_{\nu D} - \frac{(X_{\nu D} - X_i)}{c} + \Delta T(i) \quad (4)$$

---

<sup>2)</sup> Usually the beam contamination uncertainty is about 10%. A better knowledge requires a dedicated experiment for the  $K/\pi$  ratio measurement and tight control of the systematics in the Monte Carlo simulation of the beam optics.

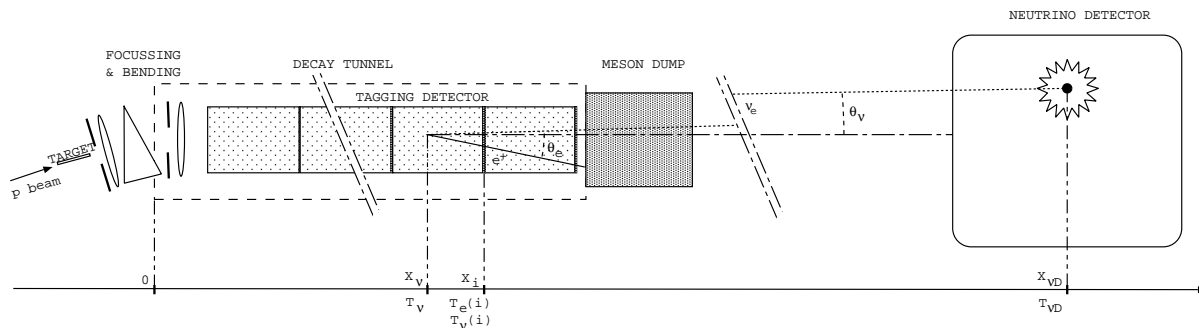


Figure 1: Conceptual layout of the experiment.

where  $X_{\nu D}$  and  $X_i$  are respectively the positions of the neutrino interaction vertex and of the  $i$ -th tagging module. The term  $\Delta T(i)$  would be zero if the neutrino crossing on the  $i$ -th tagging module would be isochronous with the positron and if  $\cos\theta_\nu = 1$ . In general  $\Delta T(i)$  depends on the beam energy and the detector geometry and it is given by

$$\Delta T(i) = \frac{(X_{\nu D} - X_i)}{c} \left( 1 - \frac{1}{\cos\theta_\nu} \right) + \frac{(X_i - X_\nu)}{c} \left[ \frac{1}{\beta_e \cos\theta_e} - \frac{1}{\cos\theta_\nu} \right] \quad (5)$$

where  $X_\nu$  is neutrino production vertex position.  $\Delta T(i)$  can be estimated on average, or even evaluated event by event when the positron direction  $\cos\theta_e$  is measured as soon as the positron is detected by more than one module.

The residual uncertainty on  $\Delta T(i)$  has to be smaller than the resolution  $\delta t$  of the time anticoincidence between  $T_{\nu D}$  and  $T_e(i)$  used to veto neutrino events.

Another condition which has to be satisfied by the time resolution  $\delta t$  of the anticoincidence, concerns the random veto due to accidental coincidence between an oscillation event and an uncorrelated positron: the time resolution should be such that  $\delta t \cdot f_t \ll 1$ , where  $f_t$  is the tagging rate.

Each tagging module operates by detecting the Cherenkov light produced by the positrons in the gas filling the decay tunnel, when the positron velocity  $\beta_e$  exceeds the Cherenkov threshold  $1/n$ , where  $n$  is the gas refractive index. The Cherenkov properties of different gases which could be suitable for our purpose will be discussed later in detail, but here we note that a gas radiator is needed in order to keep hadrons and muons below the Cherenkov threshold.

The Cherenkov photons produced along the positron path are emitted in the forward direction with an aperture angle  $\cos\Theta_\gamma = 1/(\beta_e \cdot n)$ . They all reach the tagging module almost simultaneously, filling a circular area around the positron impact point (*Cherenkov spot*) with a constant *radial* density and within a radius

$$r = d \cdot \tan\Theta_\gamma \quad (6)$$

where  $d$  is the radiator length.

It can be shown that, in the limit  $\tan\theta_e \ll 1/(n-1)$ , the following relation holds for the difference between the positron crossing time and the arrival time of the Cherenkov photons emitted at a distance  $D_\gamma$  from the tagging module

$$T_\gamma - T_e \approx \frac{D_\gamma}{c\beta_e} [n^2 - 1] \quad (7)$$

This delay of the Cherenkov photons with respect to the positrons is negligible in every practical case, compared to the neutrino-positron timing.

## 4 Experiment design

### 4.1 General layout

In this section we present a possible implementation of the anti-tagging idea, to prove its feasibility by addressing the issues of tagging rate, efficiency, neutrino flux and background. The optimization of the design and eventually the identification of alternative or complementary options is left to a more comprehensive study. All the numbers quoted in the following sections are based on the reference layout described below, and when different solutions are considered it will be explicitly stated.

The study has been performed with a full simulation of the target [34] and the magnetic optics [35] to calculate the characteristics of the secondary meson beam. The physics in the decay tunnel has been described with the JETSET Monte Carlo [36], taking into account only decays and not particle interactions.

The secondary meson beam is focussed and bent by  $15^\circ$  with a magnetic system which transports the positive charge particles into the decay tunnel. The decay tunnel is 80 m long and is instrumented with the tagging detector, which is followed by a conventional dump to absorb all particles except neutrinos.

The tagging detector consists of 25 tagging modules positioned along the tunnel. Each module is a Cherenkov threshold detector consisting of a 3 m long gas radiator followed by a planar photon detector. The gas radiator is operated slightly above the atmospheric pressure for gas purity considerations. The radiator and the photon detector are contained in a cylindrical vessel of 1 m radius with thin windows on the front and rear side. The rear window is just on the back of the photon detector. We estimate the thickness of materials traversed by the particles to be less than  $5 \cdot 10^{-3} X_0$  per tagging module.

The neutrino detector is located 810 m from the center of the decay region. For acceptance calculations, we assume a detector transverse square section of  $4 \times 4 \text{ m}^2$ .

### 4.2 Neutrino Beam

#### 4.2.1 Proton beam

A neutrino beam energy of a few GeV is suitable for a short baseline experiment with a maximum sensitivity in the range  $\Delta m_{e\mu}^2 \approx \text{few } eV^2$ .

In order to keep the tagging rate to an acceptable level, the available proton intensity should be extracted onto the target as slowly as possible. The optimal solution would be the accumulation in a storage ring with a continuous extraction. Without accumulation, the anti-tagging is feasible provided a slow extraction scheme is adopted.

At CERN the slow extraction is used both for the CPS and SPS proton accelerators. Both facilities could be exploited taking advantage of the existing decay tunnels and experimental halls. The flux estimate presented in this study is based on the assumption of a primary proton beam from the CPS accelerator with the characteristics summarized below.

We assume a spill length of 500 ms at a proton energy of 19.2 GeV. The slow extraction is less efficient than the usual fast extraction, and the requirement of minimizing the proton losses in the machine limits at present the intensity to  $10^{13}$  p/cycle. In the foreseeable future, after the LEP shutdown and before the LHC era, the CPS proton availability could probably allow to allocate up to 4 cycles of 2.4 s each, in a supercycle of 14.4 s. Then a neutrino experiment in an anti-tagged beam could run at the CPS with an intensity of  $4 \cdot 10^{13}$  protons every 14.4 seconds, with a proton on target rate of  $2 \cdot 10^{13} \text{ s}^{-1}$  during extraction.

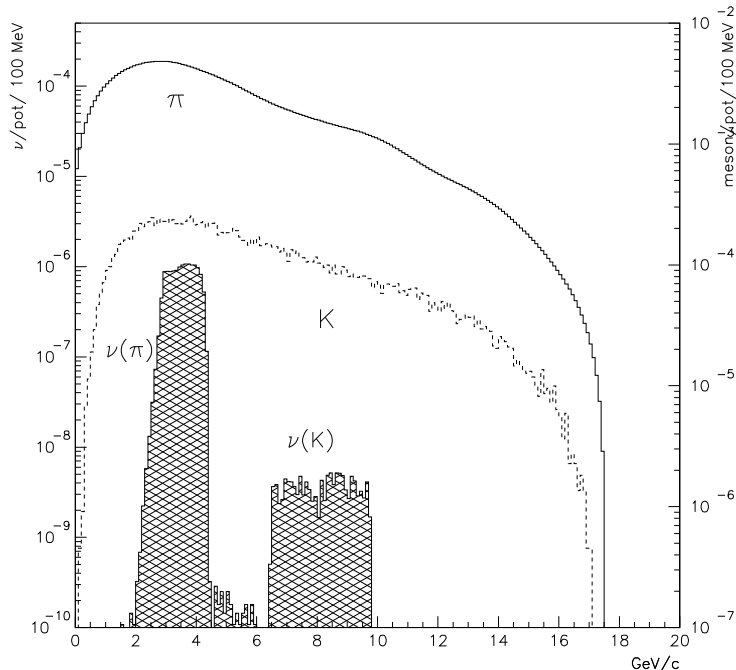


Figure 2: Meson from target (right axis) and neutrino spectra in the detector (left axis). Both are normalized to the proton on target flux.

Based on the CPS performances in the last four years, we assume a running time of 5600 hours per year devoted to physics, with an accelerator efficiency of 90%. In a two years data taking about  $1.0 \cdot 10^{20}$  protons on target could be expected.

#### 4.2.2 Target and meson beam

The secondary particles yield produced by 19.2 GeV/c protons impinging on a beryllium target is simulated using GEANT [34]. The target is a cylindrical rod, parallel to the beam, with a diameter of 3 mm and a length of 110 cm (corresponding to 2.7 absorption lengths and 3.1 radiation lengths).

Figure 2 shows the spectra of  $\pi^+$  and  $K^+$  produced in the target. A traditional horn scheme for the focussing system is incompatible with the slow extraction because it has to be operated in short pulses [37]. A magnetic system consisting of quadrupoles and dipoles can both focus and bend the meson beam from the target into the decay tunnel. In addition to the charge selection, the bending removes from the meson beam the  $K^0$  component, which is the main source of  $\nu_e$  background, and the direct photon yield from the target. The momentum acceptance of the focussing system cuts the low momentum part of the secondary beam, strongly suppressing the rate in the tagging detector due to the positrons produced by soft kaon decays and those produced in the target. A main advantage in such a focussing scheme consists in the low  $\nu_e$  background in the neutrino detector. The relative  $\nu_e$  flux is about 0.1% for a corresponding  $\nu_\mu$  yield of  $1.42 \times 10^{-5} \nu_\mu/\text{pot}$  on the neutrino detector. The  $\nu_\mu$  spectrum is shown in figure 2.

The meson beam focussing is not a critical issue, because at this energy the neutrino beam divergence is determined by the large neutrino decay angle with respect to the parent meson (24 mrad for  $\pi_{\mu 2}$  and 64 mrad for  $K_{\mu 2}$  on average). The meson beam divergence

should be small enough to contain the secondary beam inside the tagging detector.

In our simulation we assume a magnetic focussing system with an angular acceptance of  $50 \mu\text{Sr}$ , a momentum selection of  $\Delta P/P = 20\%$  centered around  $P_0 = 8.5 \text{ GeV}/c$  and a meson beam divergence of  $3 \text{ mrad}$  with a beam width of  $10 \text{ cm}$ .

As an example we have simulated [35] a possible scheme where the target is followed by a collimator slit, a quadrupolar triplet, a dipole and finally a quadrupolar doublet for the end focussing. The compactness of the end focussing section after the bending is an important feature because the presence of the magnets complicates the tagging of the meson decays. A pure quadrupolar magnetic line, with non coaxial elements, could be an alternative solution for the focussing system still allowing a bending angle [38]. An important difference with respect to the previous option, where the bending is obtained using a dipole, is the absence of the charge selection of the mesons.

The flux of minimum ionizing particles in the central region of a tagging module, where the beam intensity is maximum, is estimated to be  $180 \text{ MHz}/\text{cm}^2$ , including also the secondary particles from decays in the tunnel.

### 4.3 Tagging Detector

#### 4.3.1 Cherenkov light for tagging

Cherenkov threshold gas detectors have been used in high energy physics since a long time. The properties of a few gases at STP are reported in table 1. Helium and neon

	<i>He</i>	<i>Ne</i>	<i>H<sub>2</sub></i>	<i>CF<sub>4</sub></i>
$n - 1$ ( $10^{-4}$ units)	0.35	0.67	1.38	4.0
$\Theta_\gamma$ (mrad)	8.37	11.5	22.6	28.2
$\gamma_{thr}$	120	86	43	35
$I$ (eV)	24.6	21.6	15.4	12.
$e E_{thr}$ (GeV)	0.061	0.044	0.022	0.018
$\mu E_{thr}$ (GeV)	12.7	9.1	4.5	3.7
$\pi E_{thr}$ (GeV)	16.7	12.0	6.0	4.9
$K E_{thr}$ (GeV)	59.2	42.4	21.2	17.3
$p E_{thr}$ (GeV)	112.6	80.7	40.4	32.9

Table 1: Cherenkov properties of some gases

are natural candidates because at atmospheric pressure all positrons are above threshold, while the Cherenkov emission due to hadrons and muons can be neglected after the momentum selection. The differential Cherenkov light yield is given by

$$\frac{dN^\gamma}{dE dx} = \frac{\alpha Z^2}{\hbar c} \left( 1 - \frac{1}{\beta^2 n(E)^2} \right) \quad (8)$$

and is intrinsically small for light gases <sup>3)</sup>. The integrated light yield increases with the bandwidth and then there is a clear advantage in detecting light up to the extended ultra-violet region (EUV), defined by a photon energy  $E \lesssim 25 \text{ eV}$  ( $\lambda \gtrsim 51.2 \text{ nm}$ ). Light noble gases are particularly suitable because of their high ionization potential which determines the upper frequency for the light transmission. Appropriate EUV photon detectors have

<sup>3)</sup> For helium, in the visible spectrum, about 0.027 photons/cm are emitted at saturation.

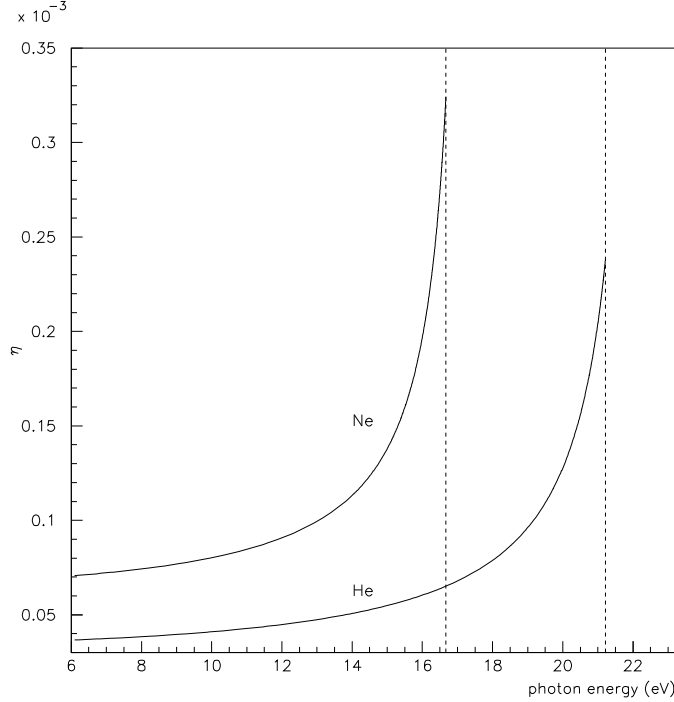


Figure 3:  $\eta = n - 1$  as a function of the Cherenkov photon energy.

to face the problem that most materials (in particular all solids) are not transparent. Solutions have been recently proposed and tested by [39, 40, 41].

In the optical region the refractive index is essentially constant but in the EUV, close to the allowed dipole transitions, the variation of the refractive index has to be taken into account in evaluating the integrated light yield from equation (8).  $\eta = n - 1$  can be calculated as a function of the photon energy by extrapolation of measurements in the optical and UV region [42]. The result is shown in figure 3 in the energy range  $6 \div 21.6$  eV for helium and  $6 \div 16.7$  eV for neon. The integrated photon/cm yield and the Cherenkov threshold for a few gas radiators are shown in figure 4. The addition of a proper “Cherenkov quencher”, i.e. traces of gas with a lower ionization potential, allows to tune the Cherenkov threshold and the light yield. The understanding, and the way to control such mechanism, can be studied in a test beam where the measurement of the light yield allows to determine experimentally, for the first time, the helium refractive index in the EUV region.

#### 4.3.2 Photon detector structure

The characteristics of a suitable photon detector can be summarized as follows:

- UV-EUV photon detection;
- time resolution  $\lesssim 1$  ns;
- spatial granularity ( $1 \div 5$  cm or less);
- low radiation length ( $\leq 0.01X_0$ );
- high rate capability;
- radiation hardness.

The required time resolution is larger than the uncertainty on the  $\Delta T(i)$  term defined in equation 5, which is about 90 ps on average.



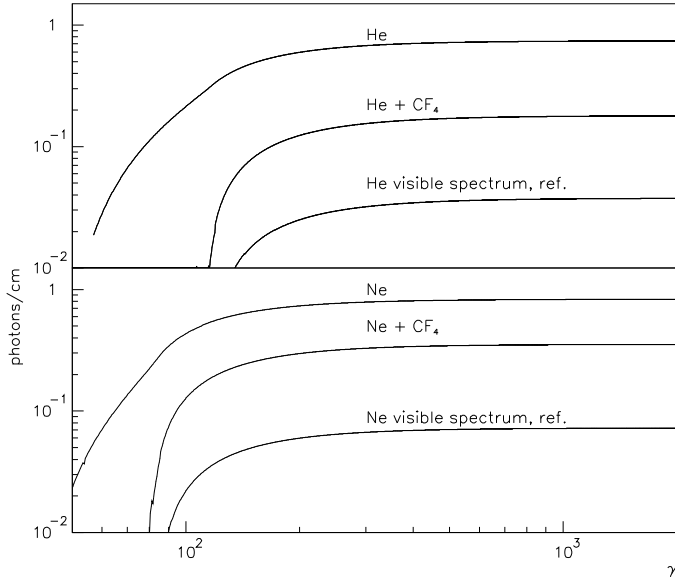


Figure 4: Cherenkov light yield as a function of  $\gamma = E/mc^2$  for He and Ne. The effect of  $CF_4$  traces is shown together with the light yield in the visible ( $350 \div 500$  nm).

In this section we show a possible detector based on the Micro-Gap Chamber (MGC) technology [43]. Other possible solutions could be studied, such as MICROMEAS [44] or MCP based EUV detectors, as well as standard detection techniques for visible light coupled to fast wavelength shifters.

The development of EUV photon detectors is particularly interesting because it could result in generic hadron blind Cherenkov detectors with fast timing and short radiator length, appealing for many applications in high energy physics. The MGC technology has already been applied to Cherenkov photon detection in the visible range [45]. Similar solutions could be adapted to detect photons in the EUV region (figure 5).

A first option consists in using *metallic window MGC*. The quartz window that delimites the drift space in UV sensitive MGC could be replaced by an ultra-thin window supported by a thicker micromesh that acts as gas separator between the drift volume and the radiator, as suggested in [46]. The ultra-thin window (about  $50$  nm) could be a metallic film with a CsI photocathode deposited by sputtering or the CsI photocathode itself. The drift distance can be  $500$   $\mu m$  or less, in order to increase the hadron blindness. The window between the drift space and the radiator allows to choose the quencher and the radiator gas mixture independently, so that the MGC can operate at the maximum gain with the most efficient radiator.

In this scheme, a positron signal can give up to  $100$  *p.e.*  $\times 5 \cdot 10^4 = 5 \cdot 10^6$  electrons collected within a Cherenkov spot of  $2.5$  cm radius ( $3.5$  cm for neon). Despite the strong suppression due to the small drift volume and the use of low  $Z$  gases, electrons can be produced by minimum ionizing particles both on the photocathode surface and, with a lower amplification, in the drift volume. In the central region of the tagging module, where the beam intensity is higher, the average signal from minimum ionizing particles on an

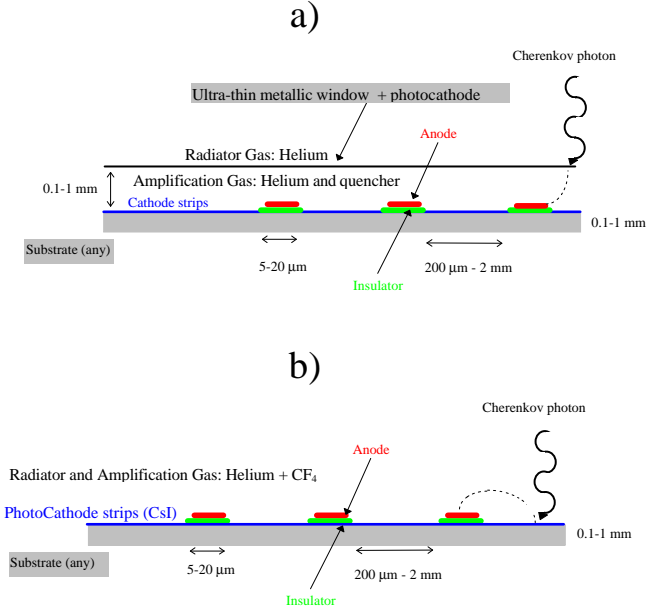


Figure 5: Two possible options for the photon detector with MGC: (a) with a thin metallic window and (b) windowless.

area corresponding to a Cherenkov spot can be estimated to be of the order of  $1 \div 2$  photoelectrons. Then the fake positrons induced by the minimum ionizing particles can be efficiently reduced by applying a pulse height threshold.

A second option consists in *windowless MGC*, where the radiator gas is the same mixture used for the amplification of the electron cascade. The photoelectrons are produced directly on the strip cathodes (see figure 5) sputtered by a thin CsI film, as already studied in many high energy physics applications [47]. CsI photocathodes in light noble gas atmosphere, when an extraction field is applied, allow very high quantum efficiencies (up to 50%) in the EUV energy range [48]. With respect to the previous configuration, the amplification occurs in a single step and is consequently smaller (about  $5 \cdot 10^3$ ). In this configuration the quencher fills the radiator volume and then quenches with high ionization potential should be preferred in order to have a higher light yield. The light transmission and the gas multiplication should be optimized by maximization of the overall signal, using for example  $CF_4$  ( $I \simeq 12 eV$ ) or DME ( $I \simeq 10 eV$ ) as quenchers.

We estimate that up to  $30 p.e. \times 5 \cdot 10^3 = 1.5 \cdot 10^5$  electrons (50 *p.e.* for Ne) are collected for an average positron. The main advantage of this option, despite of the smaller signal amplitude, is the reduced sensitivity to minimum ionizing particles, which is only due to backward emission of secondary electrons from the photocathode surface.

For the above considerations on the sensitivity to minimum ionizing particles and on the possibility to tune the Cherenkov threshold, the tagging rate is dominated by the positrons produced in the decay tunnel, and amounts to  $f_t \approx 98$  MHz. Since a positron traverses on average 6.1 modules, only 8.2 MHz are due to singles and the rest to coincidences of two or more modules.

The numbers given should be confirmed by experimental data, addressing also the issues of radiation hardness, sensitivity to minimum ionizing particles and to scintilla-

tion light, as well as the actual performances of a prototype tagging module in a beam environment.

#### 4.4 Neutrino Detector Requirements

The detector should be designed to identify a possible electron in the low multiplicity final state of a few GeV neutrino interaction. We will not address in this paper the issues of the neutrino detector in detail. The general detector requirements are

- a mass of the order of  $\sim 300 t$ ;
- a time resolution of  $\sim 1 ns$  or better;
- $e/\pi^\circ$  separation at a level of  $\leq 10^{-3}$ ;
- electron and muon identification;
- cosmics background discrimination.

A good energy resolution on neutrino interactions is an important feature for the  $\Delta m_{e\mu}^2$  measurement. To cope with these requirements several detector options are possible using technologies which are presently available or could be available with a reasonable R&D effort.

A liquid argon TPC imaging detector, characterized by an excellent separation  $e/\pi^\circ = 10^{-4}$  [49], satisfies all the requirements with the exception of the timing. This however could be provided by the detection of the scintillation light, or even better the Cherenkov light, produced in the liquid argon.

A large volume water Cherenkov detector could also be a possible neutrino detector with an intrinsically good timing.

Another viable solution consists in a conventional sandwich calorimeter, with thin ( $\lesssim 1/5 X_0$ ) absorbers and trackers, where the timing could be provided by the trackers themselves (for instance resistive plate chambers [50]) or by additional planes of fast scintillator. A different approach could be a fully active liquid scintillator calorimeter, segmented in a cell structure to provide a suitable tracking capability.

### 5 Experiment sensitivity

In this section we evaluate the  $\nu_e$  composition of the beam, the anti-tagging efficiency, and the irreducible  $\nu_e$  contamination. The possible sources of background in the  $\nu_e$  detection are discussed, in order to assess the total contamination in the oscillation search. We finally estimate the experiment sensitivity for two years data taking, and the  $\Delta m_{e\mu}^2$  measurement potential in case of a positive  $\nu_\mu \rightarrow \nu_e$  signal detection.

#### 5.1 Anti-tagged beam background

We identify the following sources of  $\nu_e$  background, of which the associated positrons are not detected by the anti-tagging detector:

- $\nu_e$  produced before the bending optics, which reach the far detector;
- decays in uninstrumented regions of the decay tunnel;
- tagging modules acceptance.

The  $\nu_e$  from decays occurring before the bending have a much softer spectrum than the  $\nu_\mu$  from the decay tunnel. Applying a loose 1.5 GeV cut on the neutrino energy, the contribution on the detector can be estimated to be  $\lesssim 0.2 \cdot 10^{-5} \nu_e/\nu_\mu$ .

The beginning of the decay tunnel, where the focussing magnets are located, and the region close to the beam dump, are potential sources of untagged  $\nu_e$ . Assuming that the photon detector of the first tagging module is positioned 6 m from the beginning of the tunnel, and that the magnets occupy the first 3 m, we estimate 42% of the positrons

produced in the magnet region cannot be detected, and this accounts for a background of  $2.7 \cdot 10^{-5} \nu_e/\nu_\mu$ . We assume that the  $\nu_e$  production in the last 50 cm of the tunnel cannot be detected. Taking also into account the decays inside the beam dump, the contribution is evaluated to be  $0.5 \cdot 10^{-5} \nu_e/\nu_\mu$ . Secondary muons from the meson decays are another source of  $\nu_e$  background, which has to be estimated considering their penetration in the dump and possible decay outside the instrumented region. However, the  $\nu_e$  contribution coming from muons escaping the decay tunnel has a soft spectrum and a broad angular distribution (due to the decay chain and the muon energy loss in matter) and from simulation it is negligible.

The geometrical inefficiency due to large angle positrons escaping undetected from the tagging modules accounts for  $2.0 \cdot 10^{-5} \nu_e/\nu_\mu$  background, including both  $K_{e3}$  and muon decays (respectively 89% and 11% of the  $\nu_e$  in the neutrino detector).

We conclude that the irreducible background is about  $5 \cdot 10^{-5} \nu_e/\nu_\mu$ , which improves by more than two orders of magnitude the  $\nu_e$  contamination with respect to conventional neutrino beams.

## 5.2 Background in the neutrino detection

The main sources of background in the detection of  $\nu_e$  interactions are  $\pi^0$  resonant and coherent production and  $\nu_\mu e$  interactions.

The cross section of coherent production, measured in the interesting energy range by the Aachen-Padova collaboration [51] and Gargamelle [52], can be estimated in about  $20 \div 40 \cdot 10^{-40} \text{cm}^2/\text{nucleon}$ , depending on the nuclear composition of the target and in agreement with the theoretical expectations [53].

Neutral pions can be produced incoherently in nucleon scattering, and fake the electron signature. The Rein and Sehgal model [54] agrees well with Gargamelle [55] data predicting  $\sigma = 8.6 \cdot 10^{-40} \text{cm}^2/\text{nucleon}$ .

The  $\nu_\mu e \rightarrow \nu_\mu e$  properties are well known from theory, and were measured by the CHARM II experiment. The cross section is typically  $1.6 \cdot 10^{-42} E_\nu (\text{GeV}) \text{cm}^2$  [56], and the characteristic kinematics can be distinguished because of the forward electron signature:  $E\theta^2 < 2m_e$ . This background can be reduced below the foreseen sensitivity by requiring, for the oscillation candidate events, a minimum angle between the observed electron and the beam axis.

## 5.3 Oscillation sensitivity

The  $\nu_\mu$  flux onto the neutrino detector is  $1.4 \cdot 10^{15} \nu_\mu$  in two years of data taking. The inclusive charged current cross section has been measured in our energy range to be  $\sigma_{\nu N} = (2.45 \pm 0.15) \cdot 10^{-38} \text{cm}^2/\text{nucleon}$  at  $\langle E_\nu \rangle = 3.6 \text{ GeV}$  [57]. This corresponds to about 36,500 neutrino interactions (corrected for accidental vetoes) in a 300 t detector. From previous considerations on background, the irreducible contamination due to the beam  $\nu_e$  component is 1.8 events. To evaluate the sensitivity in the oscillation search we restrict the sample to the range  $2 < E_\nu < 5 \text{ GeV}$ , which loosely corresponds to neutrinos produced in the pion decays: in that case 36,200  $\nu_\mu$  events are left, with a background of 1.0  $\nu_e$  events.

The overall  $\pi^0$  contamination would be  $0.14 \div 1.4$  events, depending on the separation capability ( $e/\pi^0 = 10^{-4} \div 10^{-3}$ ). We have assumed, for simplicity of normalization, 100 % detection efficiency both for signal and background, since this value strongly depends on the neutrino detector and analysis strategy. For the same reason we do not take

into account that the  $\pi^0$  and the  $\nu_\mu e \rightarrow \nu_\mu e$  backgrounds are further reduced applying the mentioned cut on the reconstructed neutrino energy.

All the relevant numbers are summarized in table 2. The exclusion plot resulting from a negative search, calculated following the procedure described in ref. [58], is shown in figure 6. The LSND region is fully covered, and part of the  $\nu_\mu \rightarrow \nu_e$  atmospheric neutrino region is also probed.

#### 5.4 $\Delta m_{e\mu}^2$ measurement

If the LSND hypothesis on  $\nu_\mu \rightarrow \nu_e$  oscillation is correct, the expected signal after two years run is  $112 \pm 40$  events, with a background of  $1.1 \div 2.4$  events. We can profit from the small uncertainty on the neutrino flight path ( $\Delta L/L \approx 3\%$  RMS) to measure  $\Delta m_{e\mu}^2$  from the energy distribution of the oscillation events. In figure 7 are reported the energy distributions of the candidates for different values of  $\Delta m_{e\mu}^2$ , in the hypothesis of a detector resolution  $\Delta E/E = 5\%/\sqrt{E(\text{GeV})}$ . In the figure are shown 224 oscillation events that could be collected with a two years “discovery extension” of the run.

Independently from  $\sin^2 2\theta_{e\mu}$ ,  $\Delta m_{e\mu}^2$  can be measured below a few  $eV^2$ , while a lower limit on  $\Delta m_{e\mu}^2$  is set for higher values. In the last case, an extension run with a higher meson momentum selection or a close smaller detector could increase the region where the  $\Delta m_{e\mu}^2$  modulation is measurable.

Proton Energy	19.2 GeV
Duration of data taking	2 years
Integrated protons on target	$1.0 \cdot 10^{20}$
Proton rate during extraction	$2 \cdot 10^{13}$ Hz
$\nu_\mu$ /pot on detector	$1.42 \times 10^{-5}$
$\nu_e/\nu_\mu$ (w/o anti-tagging)	0.1%
$\nu_e/\nu_\mu$ (with anti-tagging)	$5 \cdot 10^{-5}$
Tagging rate	$\approx 98$ MHz
Required $e/\pi^0$ separation	$10^{-4} \div 10^{-3}$
$\langle E_\nu \rangle$	3.6 GeV
$\langle L \rangle$	810 m
$\Delta L/L$ (RMS)	3%
$\nu_\mu$ events ( $\epsilon_{det} = 1$ , $E_\nu = 2 \div 5$ GeV)	36,200
$\nu_e$ background events ( $\epsilon_{det} = 1$ , $E_\nu = 2 \div 5$ GeV)	1.0
$\pi^0$ background events	$0.14 \div 1.4$
Expected $\nu_e$ oscillation events from LSND claim	112

Table 2: Main parameters and event rates.

## 6 Conclusions

We have presented the new idea of an anti-tagged  $\nu_\mu$  beam, based on the time coincidence between a positron detected in the meson decay tunnel and the neutrino interaction. The meson decay tunnel is instrumented with noble gas Cherenkov detectors, which tag the positron produced in association with the  $\nu_e$ .

We have shown the conceptual feasibility of this idea discussing a possible implementation at the CERN PS. A high energy  $\nu_\mu$  beam with an effective  $\nu_e$  contamination

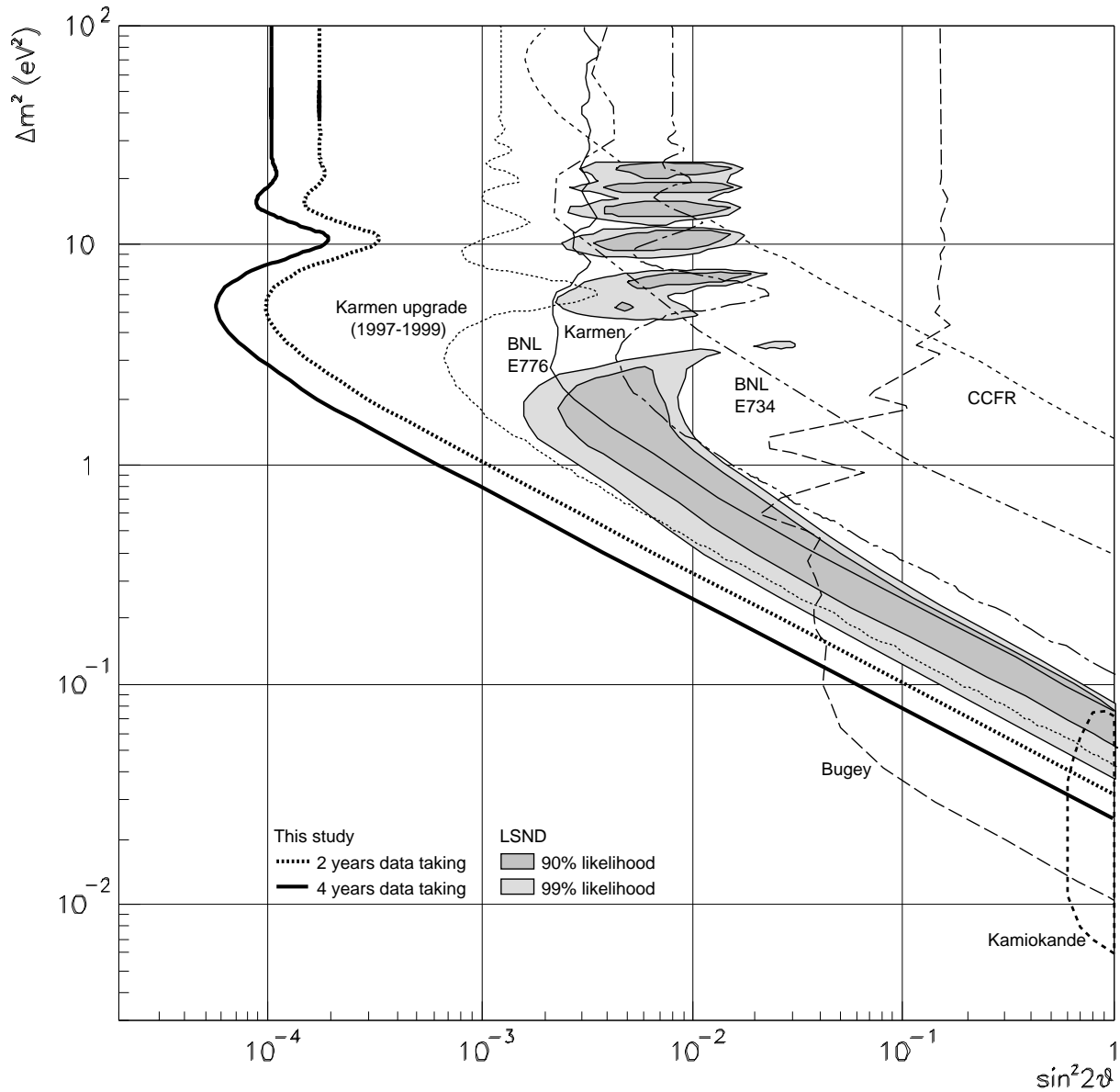


Figure 6: Exclusion plots from a negative search in a two and four years data taking period. The LSND favored regions (90% and 99% likelihood probability) are shown as well as the KAMIOKANDE inclusion plot. The present limits from BNL-E776, KARMEN, BNL-E734, Bugey, CCFR are reported. For comparison is also shown the limit that would be expected by the upgraded KARMEN detector in a three years negative search.

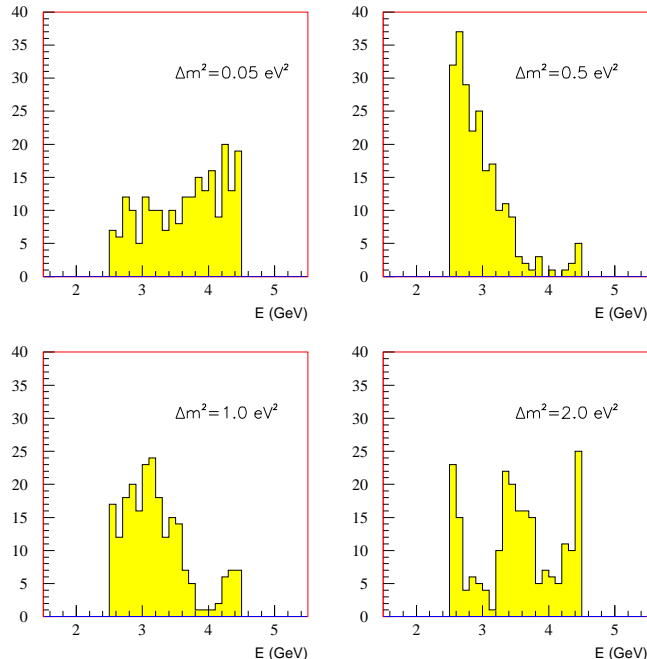


Figure 7: Spectra of oscillation events for different values of  $\Delta m_{e\mu}^2$ .

of  $5 \cdot 10^{-5}$  can be achieved resurrecting the old PS neutrino beam line. This corresponds to a reduction of the  $\nu_e$  beam contamination by more than two orders of magnitude with respect to conventional neutrino beams.

This anti-tagged  $\nu_\mu$  beam can be exploited for a *zero background* appearance search for  $\nu_\mu \rightarrow \nu_e$  oscillation, with a sensitivity which is an order of magnitude better than any present or approved experiment.

According to the LSND result, 112 oscillation events could be collected in a two years run with a background of  $1.1 \div 2.4$  events. This sample could allow an analysis of the neutrino energy modulation for an unmistakable oscillation signature and  $\Delta m_{e\mu}^2$  measurement.

## 7 Acknowledgments

It is a pleasure to warmly thank our colleagues from the CHORUS collaboration for their encouragement. We acknowledge the comments and suggestions we received from many of them and from the participants to the workshops on "Future Neutrino Experiments" at CERN. We are grateful to J.Boillot, R.Bellazzini, R.Cappi and D.J.Simon for the valuable information received in informal discussions.

## References

- [1] K.S. Hirata et al. *Phys. Rev. Lett.*, 66:9, 1991.
- [2] W. Hampel et al. *DAPNIA-SPP-96-10*, July 1996. Subm. to, *Phys. Lett.*, B.
- [3] J. N. Abdurashitov et al. *Nucl. Phys. B (Proc. Suppl.)*, 38:60, 1995.
- [4] B.T. Cleveland et al. *Nucl. Phys. B (Proc. Suppl.)*, 38:47, 1995.
- [5] Y. Fukuda et al. *Phys. Lett. B.*, 335:237, 1994.
- [6] R. Becker-Szendy et al. *Phys. Rev. Lett.*, 69:1010–1013, 1992.

- [7] C. Athanassopoulos et al. *Phys. Rev. C*, 54:2685, November 1996. LA-UR-96-1582.
- [8] J. Bahcall et al. *astro-ph/9610250*, June 1996. 17th International Conf. on Neutrino Physics and Astrophysics - NEUTRINO '96, Helsinki, Finland, 13-20 Jun 1996.
- [9] A. J. Smirnov. *hep-ph/9511239*, November 1995.
- [10] A. Dar. *astro-ph/9611014*, November 1996. 17th International Conf. on Neutrino Physics and Astrophysics - NEUTRINO '96, Helsinki, Finland, 13-20 Jun 1996.
- [11] G. Conforto et al. *hep-ph/9606226*, June 1996. UB FI 96-1, To be publ. in *Astr. Phys.*
- [12] D.R.O. Morrison. *Nucl. Phys. B, Proc. Suppl.*, 48:567, 1996.
- [13] A. De Rujula and S.L. Glashow. *hep-ph/9208223*, August 1992. HUTP-92-A038.
- [14] M. Aglietta et al. *Europhys. Lett.*, 8:611, 1989.
- [15] K. Daum et al. *WUB 95-03*, February 1995. Subm. to, *Z. Phys. C*.
- [16] W. W. M. Allison et al. *PDK-570*, November 1996. Subm. to, *Phys. Lett.*
- [17] T.K. Gaisser. *hep-ph/9611301*, November 1996. BA-96-50 and references therein.
- [18] D. Saltzberg. *Phys. Lett. B*, 355:499, April 1995.
- [19] Y. Suzuki. *presented at Int. Conf. on HEP, Warsaw*, July 1996. to be publ. in *Proceedings*.
- [20] D. Sinclair et al. *Nuovo Cimento C*, 9:308–317, 1986.
- [21] G. Ranucci et al. *Nucl. Instr. and Meth. A*, 315:229–235, 1992.
- [22] K. Eitel et al. *Proc. of the 8th Rencontres de Blois: Neutrinos, Dark Matter and the Universe*, June 1996. To be published.
- [23] C. Athanassopoulos et al. *LA-UR-96-1326*, May 1996.
- [24] S. M. Bilenyk et al. *Phys. Rev. D*, 54:1881, 1996.
- [25] J. Ellis et al. *Phys. Lett. B*, 292:189–194, 1992.
- [26] L. Wolfenstein. *hep-ph/9506352*, June 1995. CMU-HEP-9505.
- [27] K.C. Chou and Y.L. Wu. *hep-ph/9610300*, October 1996. DOE-ER-01545-675.
- [28] C. Angelini et al. *Phys. Lett. B*, 179:307, 1986.
- [29] G. Bernardi et al. *Phys. Lett. B*, 181:173, November 1986.
- [30] F. Bergsma et al. *Phys. Lett. B*, 157:469, 1985.
- [31] A. Romosan et al. *hep-ex/9611013*, November 1996. NEVIS-1529.
- [32] V. V. Ammonosov et al. *Proposal SERP-E-152*.
- [33] R. H. Bernstein et al. *Fermilab P-788*.
- [34] Application Software Group. *GEANT Detector Description and tools*, June 1993. CERN program library long writeups Q123, version 3.21.
- [35] D. C. Carey. *SLAC 246*, March 1982.
- [36] T. Sjostrand. *Computer Physics Communications*, 39:347, 1986.
- [37] S. Van der Meer. *CERN 61-07*, February 1961.
- [38] J. Panman. *CERN 83-02*, II:146, February, 10 1983. Yellow Report.
- [39] Y. Giomataris and G. Charpak. *Nucl. Inst. Meth. A*, 310:589, 1991.
- [40] Y. Giomataris et al. *Nucl. Inst. Meth. A*, 323:431, 1992.
- [41] M. Chen et al. *Nucl. Inst. Meth. A*, 346:120, 1994.
- [42] P.W. Langhoff and M. Karplus. *J. Opt. Soc. Am.*, 59:863, July 1969.
- [43] F. Angelini et al. *Nucl. Instr. and Meth.*, 335:69, October 1993.
- [44] Y. Giomataris et al. *DAPNIA/SED 95-04*, December 1995. Submitted to *Nucl. Instr. and Meth.*
- [45] F. Angelini et al. *INFN PI/AE 95/03*, May 1995. Submitted to *Nucl. Instr. and Meth.*
- [46] A. Braem et al. *CERN AT/94-33 (ET)*, September 1994.



- [47] J. Seguinot et al. *Nucl. Inst. Meth. A*, 297:133, 1990.
- [48] A. Breskin et al. *Nucl. Inst. Meth. A*, 344:163, 1994.
- [49] M. Bonesini et al. *SPSLC/I205*, June 1995. CERN/SPSLC 95-37.
- [50] R. Santonico and R. Cardarelli. *Nucl. Inst. Meth. A*, 187:377, 1981.
- [51] H. Faissner et al. *Phys. Lett. B*, 125:230, May 1983.
- [52] E. Isiksal et al. *Phys Rev. Lett.*, 52(13):1096, March 1984.
- [53] D. Rein and L.M. Sehgal. *Nucl. Phys. B*, 223:29, 1983.
- [54] D. Rein and L.M. Sehgal. *Annals of Physics*, 133:79, 1981.
- [55] W. Lerche et al. *Phys. Lett. B*, 135:45, September 1978.
- [56] P. Vilain et al. *Phys. Lett. B*, 302:351, 1993.
- [57] S. Ciampolillo et al. *Phys. Lett. B*, 84:281, June 1979.
- [58] O. Helene. *Nucl. Inst. Meth.*, 212:319, January 1983.